ISSN 2616-5880 Vol. 6, Issue 1: 44-51, DOI: 10.25236/AJMC.2025.060105

Ca-Doped Nanocrystals for Upconversion Luminescence Modulation and Their Application in Fluorescent Microspheres

Xiyan Zhu, Fei Li, Pei Jiang, Xinru Liu*

Hunan University of Science and Technology, Xiangtan, China
**Corresponding author*

Abstract: *This paper successfully synthesized $NaGdF_4$:18%Yb^{3+}/2%Er^{3+}/x%Ca^{2+}@$NaYF_4$ upconversion nanoparticles (UCNPs) with strong visible fluorescence using a solvothermal method. The upconversion luminescence intensity can be regulated by Ca^{2+} doping. Under 980 nm infrared excitation (at room temperature), the luminescence intensity gradually increases as the Ca^{2+} doping concentration increases from 0 mol% to 30 mol%. The intensity reaches its maximum at a doping concentration of 30 mol%, and then decreases gradually. Fluorescence spectra indicate that the emissions originate from two green light peaks at 540 nm and 520 nm. Transmission electron microscopy (TEM) was used to characterize the morphology of the samples, revealing that the synthesized $NaGdF_4$:18%Yb^{3+}/2%Er^{3+}/x%Ca^{2+} @$NaYF_4$ upconversion nanocrystals have a hexagonal phase, uniform morphology, good particle dispersion, and an average particle size of approximately 60 nm. Based on these findings, nanocrystals with a 30 mol% doping concentration were selected for further processing and coating to enhance the luminescence intensity.*

Keywords: *Upconversion luminescence; Core shell nanocrystals; Ca^{2+}doping; coating*

1. Introduction

Upconversion (UC) materials are luminescent materials that can absorb low-energy light and emit high-energy light. In 1959, Halsted [1] observed green emission at 525 nm when polycrystalline ZnS was excited by 960 nm infrared light. In 1966, Auzel accidentally discovered during the study of tungstate-based sodium glasses that when Yb^{3+} ions were doped into the material, the visible light emission intensity from Er^{3+}, Tm^{3+}, and Ho^{3+} ions increased by about two orders of magnitude when excited by infrared light. This phenomenon, where lower-energy photons are absorbed to emit higher-energy photons, is known as UC luminescence, also referred to as the anti-Stokes effect [2-10].Due to the unique genetic characteristics of cancer, it remains an unresolved challenge in the medical field. Traditional treatments often have side effects and limited efficacy. In contrast, UC nanomaterials can effectively reduce the damage caused by conventional treatments to the biological system, enhance the targeted delivery of drugs, and help eliminate cancerous cells. C-S type UCNPs, due to their unique advantages, are commonly used in photothermal therapy, drug delivery, and photodynamic therapy[11-20].

Rare-earth UC nanomaterials, due to their unique optical properties, hold broad application prospects in fields such as imaging, probes, and particularly biomedicine. However, due to current research limitations, the luminescence efficiency of rare-earth UCNPs remains relatively low, which significantly hinders the development of UC luminescent materials. Therefore, enhancing the luminescence efficiency of UC materials has become one of the key issues to address in current research [21-33].

In this study, a series of core-shell structured $NaGdF_4$:18%Yb^{3+}/2%Er^{3+}/x%Ca^{2+}@$NaYF_4$ fluorescent nanoparticles were prepared using a solvothermal method. During the experiment, the doping level of Ca^{2+} was varied to adjust the luminescence intensity of the UCNPs $NaGdF_4$:Yb^{3+}/Er^{3+}/ Ca^{2+}@$NaYF_4$. By introducing Ca^{2+} as a dopant into the UCNPs lattice, it was found that as the Ca^{2+} concentration gradually increased, the UC luminescence intensity of the UCNPs was significantly enhanced, reaching its maximum at a doping concentration of 30 mol%. This enhancement is likely attributed to the change in the local crystal field symmetry of $NaGdF_4$ and the improvement in the nanocrystals' crystallinity.

ISSN 2616-5880 Vol. 6, Issue 1: 44-51, DOI: 10.25236/AJMC.2025.060105

2. Experimental

2.1. Materials and characteristics

The rare earth oxides used in this experiment all have a purity of 99.99%. A corresponding amount of rare earth oxide was dissolved in hydrochloric acid, and deionized water was added to adjust the solution to the required concentration, preparing rare earth chlorides $GdCl_3$ (Yb, Er, Ca, Y) aqueous solutions. Oleic acid (OA) (90%), octadecene (ODE) (90%), NaOH (98%), NH_4F (98%), methanol (99%), polyethylene glycol (90%), ethanol (90%), and cyclohexane (90%) were all purchased from Sigma-Aldrich and used as starting materials without further purification.

2.2. Experimental Steps

2.2.1. Synthesis of $NaGdF_4:Yb^{3+}/Er^{3+}/Ca^{2+}$ Core Structure

$NaGdF_4:Yb^{3+}/Er^{3+}/xCa^{2+}$ nanoparticles were synthesized using a conventional solvothermal method. $GdCl_3$ aqueous solution (x mmol = percentage * 0.2 mmol), $YbCl_3$ aqueous solution (0.036 mmol), $ErCl_3$ aqueous solution (0.004 mmol), and $CaCl_2$ (y mmol = percentage * 0.2 mmol) were added to a 50 mL two-neck round-bottom flask (A), which also contained 12 mL of octadecene (ODE) and 4 mL of oleic acid (OA). The resulting mixture was heated to 160°C and stirred continuously to remove residual water and oxygen. Simultaneously, a 5 mL methanol solution of NH_4F (1.5 mmol) and NaOH (1 mmol) was added to another flask (B) containing 4 mL of OA and 4 mL of ODE. This mixture was stirred at 50°C for 30 min, then heated to 90°C and stirred for an additional 60 min. After the methanol had evaporated from the reaction mixture, the solutions from flask A and flask B were combined and stirred for 30 min. The mixture was then allowed to cool naturally to room temperature for storage.

2.2.2. Synthesis of $NaYF_4$ Shell

$NaYF_4$ nanoparticles were synthesized using a conventional solvothermal method. YCl_3 aqueous solution (0.2 mmol) was added to a 50 mL two-neck round-bottom flask (A) containing 12 mL of octadecene (ODE) and 4 mL of oleic acid (OA). The resulting mixture was heated to 160°C and stirred continuously to remove residual water and oxygen. Meanwhile, in another flask (B) containing 4 mL of OA and 4 mL of ODE, a 5 mL methanol solution of NH_4F (1.5 mmol) and NaOH (1 mmol) was added. This mixture was stirred at 50°C for 30 min, then heated to 90°C and stirred for an additional 60 min. Once the methanol had evaporated from the reaction mixture, the solutions from flask A and flask B were combined and stirred for 30 min. The mixture was then allowed to cool naturally to room temperature for storage.

2.2.3. Synthesis of $NaGdF_4:Yb^{3+}/Er^{3+}/Ca_{2+}@NaYF_4$ Core-Shell Nano Structure

The synthesized $NaGdF_4:Yb^{3+}/Er^{3+}/Ca^{2+}$ core and $NaYF_4$ shell were added to a 50 mL flask containing 15 mL of octadecene (ODE) and 15 mL of oleic acid (OA). Argon gas was continuously bubbled into the flask to isolate the reaction from air. The mixture was stirred and heated to 160°C, maintaining this temperature for 30 min to remove water and oxygen from the solution, resulting in a uniform and clear yellow solution. Afterward, the temperature was increased to 210°C and maintained for an appropriate time to ensure the complete removal of residual water. Finally, the solution was rapidly heated (within 15 min) to 310 °C and kept at this temperature for 120 min.

After the reaction, the temperature controller was turned off, and a brown transparent mixture was obtained. The mixture was cooled to room temperature under an argon atmosphere. Anhydrous ethanol was then added in a volume ratio of approximately 1:1. The mixture was centrifuged at 10,000 rpm for 5 min, and the brown product was collected. The product was washed three times with cyclohexane and anhydrous ethanol. Finally, the product was dispersed in 8 mL of cyclohexane and stored for further use.

2.2.4. Preparation of UCNPs Coated with Polystyrene (PS) Spheres

Select the nanocrystals with a doping concentration of 30 mol%, and perform oleic acid removal treatment on the synthesized $NaGdF_4:Yb^{3+}/Er^{3+}/Ca^{2+}@NaYF_4$. In a mixture of 5 μL of polystyrene microsphere dispersion and 200 μL of butanol, add 300-600 μL of the solution containing the ligand-free nanoparticles. The mixture was left to stand at room temperature for 120 min. Then, centrifuge at 6000 rpm for 5 min, wash the product with deionized water, and disperse the final composite in deionized water for further use.

ISSN 2616-5880 Vol. 6, Issue 1: 44-51, DOI: 10.25236/AJMC.2025.060105

2.3. Description

A series of $NaGdF_4$:18%Yb^{3+}/2%Er^{3+}/Ca^{2+}@$NaYF_4$ core-shell nanoparticles with different Ca^{2+} doping concentrations were synthesized. Clearly, the introduction of Ca^{2+} doping significantly enhanced the luminescence of the UC fluorescent nanoparticles, and the change in emission intensity with increasing Ca^{2+} concentration was visibly noticeable. As the Ca^{2+} doping concentration increased from 0 to 30 mol%, the luminescence intensity of the UCNPs began to increase. However, when the Ca^{2+} doping concentration was further increased to 40 mol%, the emission intensity of the UC fluorescent nanoparticles started to decrease.

2.4. Characterization of Nanoparticles

The size and morphology of $NaGdF_4$:18%Yb^{3+}/2%Er^{3+}/ Ca^{2+}@$NaYF_4$ core-shell nanoparticles with a doping concentration of 30 mol% Ca^{2+}, where the luminescence intensity reached its maximum value, were measured using a Hitachi H-7650c Transmission Electron Microscope (TEM) operating at 80 kV. The emission spectra of the nanoparticles with different Ca^{2+} doping concentrations were measured using a Hitachi F-2700 spectrophotometer. A 980 nm laser was used as the excitation source, and the emission spectra were recorded in the range of 300 to 700 nm. Up-conversion luminescence images were captured using a camera. All the experiments were conducted at room temperature.

3. Results and discussion

3.1. Upconversion Luminescence of $NaGdF_4$ Nanoparticles

This study investigates the synthesis of luminescent $NaGdF_4$ nanocrystals using a solvothermal method. The doping agents play a crucial role in controlling the luminescence intensity of the $NaGdF_4$ nanoparticles.

Under excitation by a 980 nm laser, the UC luminescence intensity of $NaGdF_4$:18%Yb^{3+}/2%Er^{3+}/xCa^{2+}@ $NaYF_4$ nanocrystals was measured using a Hitachi FL2700 spectrophotometer, with other relevant parameters controlled. As shown in Figures 1(a-b), the UC luminescence spectrum of $NaGdF_4$:18%Yb^{3+}/2%Er^{3+}/Ca^{2+}@$NaYF_4$ nanocrystals is primarily composed of two emission bands. From Figure 2, it can be seen that in the Yb^{3+}-doped nanocrystals, the emission process of Er^{3+} ions occurs through energy transfer between Yb^{3+} and Er^{3+} ions. First, Yb^{3+} ions absorb the 980 nm laser, transitioning from the $^2F_{7/2}$ to the $^2F_{5/2}$ state. Then, Yb^{3+} ions transfer their excited energy to nearby Er^{3+} ions via non-radiative relaxation or energy transfer. After absorbing this energy, the Er^{3+} ions release photons through a series of radiative transitions, producing light at specific wavelengths. The green emission peak centered at 520 nm corresponds to the Er^{3+} $^2H_{11/2} \rightarrow {}^4I_{15/2}$ electronic transition, and the strong green emission peak centered at 540 nm is associated with the Er^{3+} $^4S_{3/2} \rightarrow {}^4I_{15/2}$ electronic transition. Additionally, the red emission peak centered at 653 nm corresponds to the Er^{3+} $^4F_{9/2} \rightarrow {}^4I_{15/2}$ electronic transition, although it is very weak. As shown in Figure 1(a), this red emission is only detectable at the highest emission intensity.

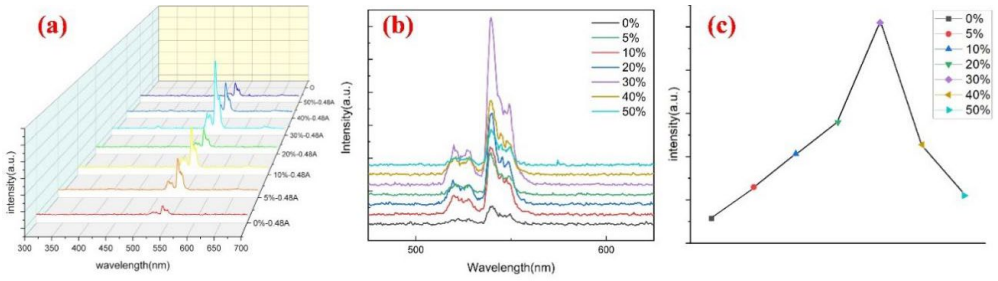

Figure 1: (a-b) UC fluorescence spectra of $NaYF_4$:Ca^{2+}/18%Yb^{3+}/2%Er^{3+}@ $NaGdF_4$ nanoparticles (the doping concentration of Ca^{2+} is 0, 5, 10, 20, 30, 40, 50 mol%) under 980 nm laser excitation (at the same nanoparticle concentration) at room temperature.(c) Peak comparison of $NaYF_4$:Ca^{2+}/18%Yb^{3+}/2%Er^{3+}@ $NaGdF_4$ nanoparticles (the doping concentration of Ca^{2+} is 0, 5, 10, 20, 30, 40, 50 mol%) at the 540 nm emission wavelength.

ISSN 2616-5880 Vol. 6, Issue 1: 44-51, DOI: 10.25236/AJMC.2025.060105

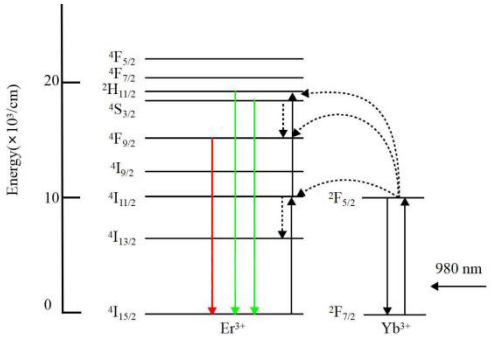

Figure 2: Energy level diagram of Er^{3+} ions.

As can be clearly observed in Figure 1(c), under excitation by the near-infrared 980 nm laser, the emission intensity of the Ca^{2+}-doped nanocrystals is higher than that of the undoped nanocrystals. Furthermore, as the doping concentration of Ca^{2+} increases, the emission intensity is further enhanced. The highest brightness is achieved when the Ca^{2+} doping concentration reaches 30%. However, after the doping concentration reaches 30%, further increases in the doping concentration result in a decrease in the luminescence intensity. To make this effect more intuitive and easier to observe, a camera was used to capture images of the $NaGdF_4$:18%Yb^{3+}/2%Er^{3+}/x%Ca^{2+}@$NaYF_4$ nanoparticles with Ca^{2+} doping concentrations ranging from 0% to 50%. These images are shown in Figure 3 .

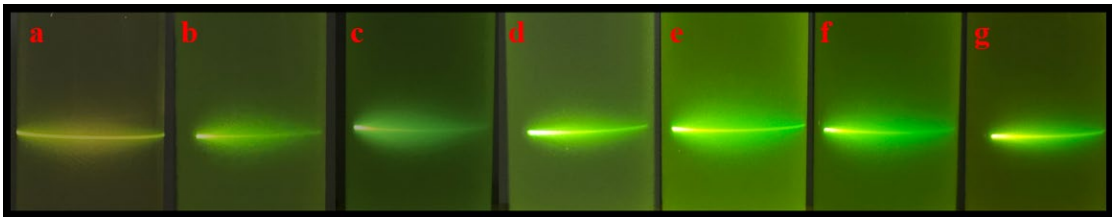

Figure 3: The luminescent images of $NaGdF_4$:18%Yb^{3+}/2%Er^{3+}/x%Ca^{2+}@$NaYF_4$ nanocrystals dispersed in cyclohexane solution under 980 nm laser irradiation (with the same nanoparticle concentration) are shown below. Panels (a-g) represent the doping concentrations of Ca^{2+} at 0%, 5%, 10%, 20%, 30%, 40%, and 50% respectively.

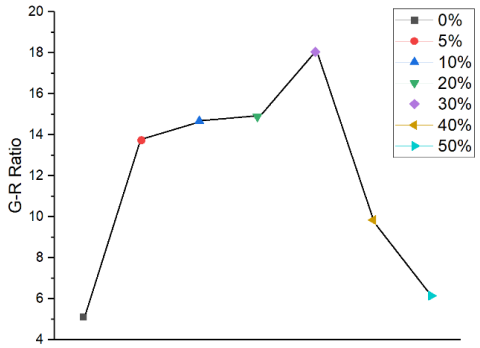

Figure 4: Effect of Ca^{2+} ion doping concentration on the green-red emission intensity ratio.

Figure 4 shows the relationship between the integral green-red emission intensity and the Ca^{2+} doping concentration. From Figure 4, it is clear that the green-red luminescence intensity ratio changes with the increasing concentration of Ca^{2+} ions. As the Ca^{2+} doping concentration increases, the overall trend of the green-red emission intensity first increases and then decreases. The green-red emission intensity ratio reaches its maximum when the Ca^{2+} doping concentration is 30%.

ISSN 2616-5880 Vol. 6, Issue 1: 44-51, DOI: 10.25236/AJMC.2025.060105

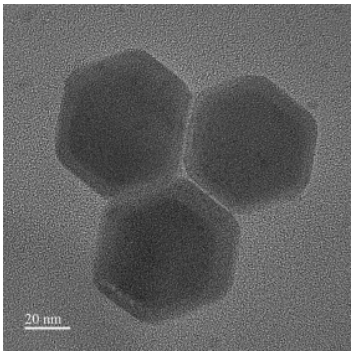

Figure 5: TEM image of $NaGdF_4$:18%Yb^{3+}/2%Er^{3+}/30%Ca^{2+}@$NaYF_4$ nanocrystals.

To reveal the morphology and size of the synthesized $NaGdF_4$ nanocrystals, transmission electron microscopy (TEM) and high-resolution TEM (HRTEM) were used for characterization. The UC fluorescent nanoparticles with the highest luminescence intensity (i.e., x = 30%) were selected for observation, as shown in Figure 5. From the TEM images, it can be seen that the $NaGdF_4$:18%Yb^{3+}/2%Er^{3+}/x%Ca^{2+}@$NaYF_4$ nanocrystals exhibit a nearly hexagonal phase, with a monodispersed and uniform structure, demonstrating good crystallinity. The average size of the core is approximately 50 nm, while after the coating of the shell, the average particle size increases to around 60 nm.

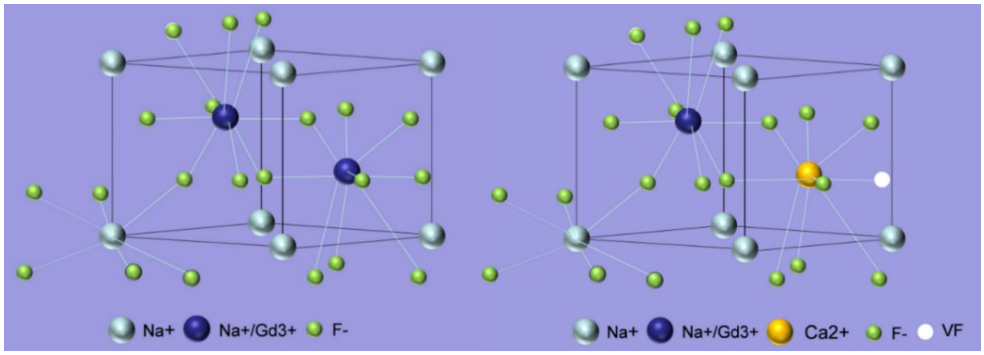

Figure 6: Crystal structure of $NaGdF_4$: Yb^{3+}/Er^{3+}/ Ca^{2+}@$NaYF_4$.

From the crystal structure perspective, β-$NaGdF_4$ is an unordered crystal where Na^+ and Gd^{3+} cations are randomly distributed at the same lattice positions, resulting in multiple active sites for the doped Ln^{3+} ions. As shown in Figure 6, when Ca^{2+} ions are introduced into the $NaGdF_4$ host, they substitute for Gd^{3+} ions in the lattice. To balance the charge, an additional F^- ion is introduced. This modification of the $NaGdF_4$ crystal structure caused by Ca^{2+} doping further diversifies the active sites for the Ln^{3+} ions. The doping of Ca^{2+} ions into the $NaGdF_4$ lattice reduces the symmetry of the local crystal field around the Er^{3+} ions, thereby increasing the probability of electronic transitions, which ultimately changes the luminescence intensity. At low concentrations of Ca^{2+} doping, Ca^{2+} ions tend to substitute for Gd^{3+} ions in the lattice, leading to lattice contraction. This contraction reduces the symmetry of the local crystal field around Er^{3+} ions, which increases the luminescence intensity. The presence of Yb^{3+} and Er^{3+} ions at multiple independent sites within the host increases the energy transfer process from Yb^{3+} to Er^{3+}, significantly enhancing the probability of highly efficient resonance or near-resonance processes, resulting in a substantial enhancement of the UC luminescence in the Ca^{2+}-doped samples. On the other hand, it has been established that the UC emission of Ln^{3+} doped materials depends on the 4f intra-configurational transition probability, which is significantly influenced by the local crystal field environment of the Ln^{3+} ions. A lower crystal symmetry typically favors higher UC efficiency, as the mixing of the f-states of Ln^{3+} ions with higher electronic configurations becomes more pronounced, effectively breaking the forbidden 4f-4f transitions. The formation of F^- vacancies in the host (due to the substitution of Gd^{3+} by Ca^{2+}) reduces the symmetry of the local crystal field around Yb^{3+} and Er^{3+} ions, which helps break the forbidden transitions of Ln^{3+} ions and enhances Er^{3+} UC luminescence. However, when the Ca^{2+} doping concentration exceeds 30%, the luminescence intensity begins to decrease. This is likely because, at concentrations higher than 30%, an increasing number of Ca^{2+} ions occupy interstitial sites in the lattice, leading to an increase in the symmetry of the lattice. As a result, the symmetry of the local crystal field around Er^{3+} ions also gradually increases, which ultimately leads to a reduction in the luminescence intensity. Additionally, the continuous introduction of Ca^{2+} also brings an excess of F^- ions,

ISSN 2616-5880 Vol. 6, Issue 1: 44-51, DOI: 10.25236/AJMC.2025.060105

which may cause fluorescence quenching. Furthermore, the higher doping concentration leads to an increase in surface-adsorbed groups, which also contributes to the reduction in luminescence intensity.

3.2. The Effect of Coating Nanocrystals with Polystyrene (PS) Microspheres

Nanocrystal coating can enhance the chemical stability of polystyrene (PS) spheres under various environmental conditions. The coating layer improves the hydrophilic or hydrophobic properties of the PS surface and enhances its resistance to ultraviolet radiation and oxidation. Additionally, it imparts specific functionalities such as catalytic activity, adsorption capacity, or optical properties, thereby broadening its applications in fields like electronics and optics. Figure 7 illustrates the coating effect:

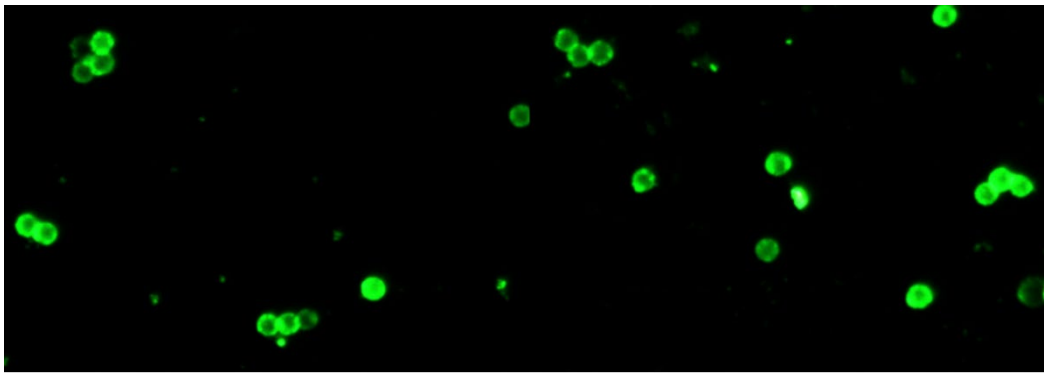

Figure 7: Effect of UCNPs Coating on PS Spheres.

Figure 8 shows the fluorescence spectra of UCNPs and UCNPs coated with PS microspheres under 980 nm near-infrared laser excitation. It is observed that the emission intensity is significantly enhanced after the UCNPs are coated with PS microspheres. The increase in emission intensity makes the sensor more sensitive to temperature changes, allowing it to detect even small temperature variations, thus enabling more precise temperature measurements. The higher emission intensity can effectively enhance the signal strength, reduce the relative influence of background noise, and improve the signal-to-noise ratio, making the measurement results more reliable. The enhanced fluorescence intensity also improves the sensor's performance across different temperature ranges, ensuring stable operation even in high or low-temperature environments.

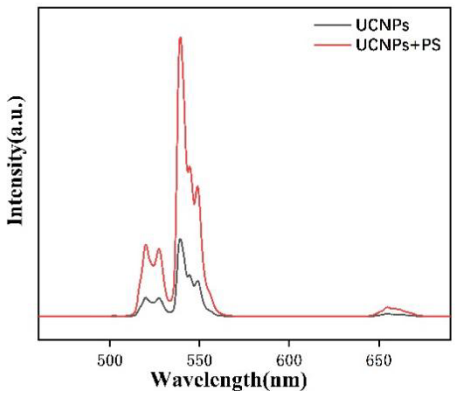

Figure 8: UC Emission Spectra of UCNPs and UCNPs+PS under 980 nm Excitation.

4. Conclusion

In summary, this experiment successfully synthesized a series of Ca^{2+}-doped $NaGdF_4$ UC nanocrystals using a solvothermal method, based on the core-shell structure of $NaGdF_4$:Yb^{3+}/Er^{3+}@$NaYF_4$.

Under the same single-wavelength infrared light source (980 nm) excitation power density, the luminescence intensity of Ca^{2+}-doped $NaGdF_4$:18%Yb^{3+}/2%Er^{3+}/x%Ca^{2+}@$NaYF_4$ was significantly enhanced compared to the undoped C-S-type UCNPs. By adjusting the doping concentration of Ca^{2+}, the luminescence intensity of the nanocrystals was observed. Experimental observations showed that when the Ca^{2+} doping concentration reached 30%, the luminescence was the strongest, both visually and in the

ISSN 2616-5880 Vol. 6, Issue 1: 44-51, DOI: 10.25236/AJMC.2025.060105

captured images. Moreover, the room-temperature UC fluorescence spectrum (under 980 nm laser diode excitation, with the same nanoparticle concentration) further confirmed that the fluorescence performance at a doping concentration of 30% was approximately 10 times stronger than that of the undoped nanocrystals. TEM imaging was performed on the UC nanocrystals with the highest luminescence intensity (i.e., with 30% Ca^{2+} doping), and the particle morphology was found to be uniform. The experimental results suggest that the introduction of Ca^{2+} altered the crystal structure, which in turn led to the change in luminescence intensity. To further enhance the sensitivity, signal-to-noise ratio, and measurement range of UCNP-based temperature sensors, an exploration of the coating of the nanocrystals with PS spheres was conducted. By improving the luminescence intensity, the application of these nanocrystals in temperature sensors was significantly enhanced, meeting stricter technical requirements. This makes them widely applicable in fields such as biomedical monitoring, industrial monitoring, and environmental sensing.

References

[1] Halsted, R. E., Apple, E. F., & Prener, J. S. (1959). Two-State optical excitation in sulfide phosphors. Physical Review Letters, 2(10), 420.

[2] Auzel, F. E. (1973). Materials and devices using double-pumped-phosphors with energy transfer. Proceedings of the IEEE, 61(6), 758-786.

[3] Liu, Y., Tu, D., Zhu, H., Li, R., Luo, W., & Chen, X. (2010). A strategy to achieve efficient dual-mode luminescence of Eu3+ in lanthanides doped multifunctional NaGdF4 nanocrystals. Advanced Materials, 22(30), 3266-3271.

[4] Peng, H. Y., Ding, B. B., Ma, Y. C., Sun, S. Q., Tao, W., Guo, Y. C., ... & Qian, H. S. (2015). Sequential growth of sandwiched $NaYF_4$: Yb/Er@ $NaYF_4$: Yb@$NaNdF_4$: Yb core–shell–shell nanoparticles for photodynamic therapy. Applied Surface Science, 357, 2408-2414.

[5] Ansari, A. A., Parchur, A. K., Nazeeruddin, M. K., & Tavakoli, M. M. (2021). Luminescent lanthanide nanocomposites in thermometry: Chemistry of dopant ions and host matrices. Coordination Chemistry Reviews, 444, 214040.

[6] Ding, B. B., Liu, K., Zhang, F., Wang, Y., Cheng, S., Lu, Y., & Qian, H. S. (2015). Facile synthesis of β-$NaGdF_4$: Yb/Er@ CaF_2 nanoparticles with enhanced upconversion fluorescence and stability via a sequential growth process. CrystEngComm, 17(31), 5900-5905.

[7] Hou, S., Zou, Y., Liu, X., Yu, X., Liu, B., Sun, X., & Xing, Y. (2011). CaF_2 and CaF_2: Ln^{3+}(Ln= Er, Nd, Yb) hierarchical nanoflowers: hydrothermal synthesis and luminescent properties. CrystEngComm, 13(3), 835-840.

[8] Liang, M. Y., Zhao, B., Xiong, Y., Chen, W. X., Huo, J. Z., Zhang, F., ... & Li, Y. (2019). A "turn-on" sensor based on MnO 2 coated UCNPs for detection of alkaline phosphatase and ascorbic acid. Dalton Transactions, 48(43), 16199-16210.

[9] Su, Y., Liu, X., Lei, P., Xu, X., Dong, L., Guo, X., ... & Zhang, H. (2016). Core–shell–shell heterostructures of α-$NaLuF_4$: Yb/Er@ $NaLuF_4$: Yb@ MF_2 (M= Ca, Sr, Ba) with remarkably enhanced upconversion luminescence. Dalton Transactions, 45(27), 11129-11136.

[10] Zhao, J., Zhu, Y. J., Wu, J., & Chen, F. (2015). Microwave-assisted solvothermal synthesis and upconversion luminescence of CaF_2: Yb^{3+}/Er^{3+} nanocrystals. Journal of colloid and interface science, 440, 39-45.

[11] Ma, C., Xu, X., Wang, F., Zhou, Z., Wen, S., Liu, D., ... & Jin, D. (2016). Probing the interior crystal quality in the development of more efficient and smaller upconversion nanoparticles. The journal of physical chemistry letters, 7(16), 3252-3258.

[12] Wen, S., Li, D., Liu, Y., Chen, C., Wang, F., Zhou, J., ... & Jin, D. (2022). Power-dependent optimal concentrations of Tm^{3+} and Yb^{3+} in upconversion nanoparticles. The Journal of Physical Chemistry Letters, 13(23), 5316-5323.

[13] Gao, W., Han, S., Wang, B., Sun, Z., Lu, Y., Han, Q., ... & Dong, J. (2022). Single-layer gold nanoparticle film enhances the upconversion luminescence of a single $NaYbF_4$: 2% Er^{3+} microdisk. Journal of Alloys and Compounds, 900, 163493.

[14] Pandurangappa, C., Lakshminarasappa, B. N., & Nagabhushana, B. M. (2010). Synthesis and characterization of CaF2 nanocrystals. Journal of alloys and compounds, 489(2), 592-595.

[15] Wang, S., Xi, W., Wang, Z., Zhao, H., Zhao, L., Fang, J., ... & Sun, L. (2020). Nanostructures based on vanadium disulfide growing on UCNPs: simple synthesis, dual-mode imaging, and photothermal therapy. Journal of Materials Chemistry B, 8(27), 5883-5891.

[16] Zhao, J., Hu, Y., wei Lin, S., Resch-Genger, U., Zhang, R., Wen, J., ... & Ou, J. (2020). Enhanced luminescence intensity of near-infrared-sensitized upconversion nanoparticles via Ca^{2+} doping for a nitric oxide release platform. Journal of Materials Chemistry B, 8(30), 6481-6489.

ISSN 2616-5880 Vol. 6, Issue 1: 44-51, DOI: 10.25236/AJMC.2025.060105

[17] Lin, M., Cheng, S., Wu, X., Zhan, S., & Liu, Y. (2021). Optical temperature sensing based on upconversion nanoparticles with enhanced sensitivity via dielectric superlensing modulation. Journal of Materials Science, 56, 10438-10448.

[18] Li, D., Shao, Q., Dong, Y., & Jiang, J. (2014). Anomalous temperature-dependent upconversion luminescence of small-sized $NaYF_4$: Yb^{3+}, Er^{3+} nanoparticles. The Journal of Physical Chemistry C, 118(39), 22807-22813.

[19] Lu, E., Pichaandi, J., Arnett, L. P., Tong, L., & Winnik, M. A. (2017). Influence of Lu^{3+} doping on the crystal structure of uniform small (5 and 13 nm) $NaLnF_4$ upconverting nanocrystals. The Journal of Physical Chemistry C, 121(33), 18178-18185.

[20] Li, Z., Lv, S., Wang, Y., Chen, S., & Liu, Z. (2015). Construction of LRET-based nanoprobe using upconversion nanoparticles with confined emitters and bared surface as luminophore. Journal of the American Chemical Society, 137(9), 3421-3427.

[21] Jiang, T., Qin, W., & Zhao, D. (2012). Size-dependent upconversion luminescence in CaF_2: Yb^{3+}, Tm^{3+} nanocrystals. Materials Letters, 74, 54-57.

[22] Chan, E. M., Han, G., Goldberg, J. D., Gargas, D. J., Ostrowski, A. D., Schuck, P. J., ... & Milliron, D. J. (2012). Combinatorial discovery of lanthanide-doped nanocrystals with spectrally pure upconverted emission. Nano letters, 12(7), 3839-3845.

[23] Fischer, S., Mehlenbacher, R. D., Lay, A., Siefe, C., Alivisatos, A. P., & Dionne, J. A. (2019). Small alkaline-earth-based core/shell nanoparticles for efficient upconversion. Nano letters, 19(6), 3878-3885.

[24] Lei, L., Liu, E., Wang, Y., Hua, Y., Zhang, J., Chen, J., ... & Xu, S. (2021). Amplifying upconversion by engineering interfacial density of state in sub-10 nm colloidal core/shell fluoride nanoparticles. Nano Letters, 21(24), 10222-10229.

[25] Lei, L., Chen, D., Huang, P., Xu, J., Zhang, R., & Wang, Y. (2013). Modifying the size and uniformity of upconversion Yb/Er: $NaGdF_4$ nanocrystals through alkaline-earth doping. Nanoscale, 5(22), 11298-11305.

[26] Pedroni, M., Piccinelli, F., Passuello, T., Giarola, M., Mariotto, G., Polizzi, S., ... & Speghini, A. (2011). Lanthanide doped upconverting colloidal CaF_2 nanoparticles prepared by a single-step hydrothermal method: toward efficient materials with near infrared-to-near infrared upconversion emission. Nanoscale, 3(4), 1456-1460.

[27] Quintanilla, M., Hemmer, E., Marques-Hueso, J., Rohani, S., Lucchini, G., Wang, M., ... & Vetrone, F. (2022). Cubic versus hexagonal–phase, size and morphology effects on the photoluminescence quantum yield of $NaGdF_4$: Er^{3+}/Yb^{3+} upconverting nanoparticles. Nanoscale, 14(4), 1492-1504.

[28] Zhou, Y., Cheng, Y., Xu, J., Lin, H., & Wang, Y. (2021). Thermo-enhanced upconversion luminescence in inert-core/active-shell UCNPs: the inert core matters. Nanoscale, 13(13), 6569-6576.

[29] Liu, Q., Zhang, Y., Peng, C. S., Yang, T., Joubert, L. M., & Chu, S. (2018). Single upconversion nanoparticle imaging at sub-10 W cm^{-2} irradiance. Nature photonics, 12(9), 548-553.

[30] Dong, B., Wu, X., Zhan, S., Nie, G., Wu, S., Cheng, S., ... & Liu, Y. (2020). Observation of high efficient photothermal conversion of sub-10nm Au nanoparticles coated on upconversion nanoparticles. Optical Materials, 101, 109665.

[31] Yu, X., Xia, Q., Liu, P., & Xu, Y. (2023). In-situ confinement of ultra-small $NaYF_4$: Yb^{3+}/Er^{3+} UCNPs as multifunctional ratiometric thermometer and optical heater. Optical Materials, 142, 114069.

[32] Cao, C., Qin, W., Zhang, J., Wang, Y., Wang, G., Wei, G., ... & Jin, L. (2008). Up-conversion white light of Tm^{3+}/Er^{3+}/Yb^{3+} tri-doped CaF_2 phosphors. Optics Communications, 281(6), 1716-1719.

[33] Zhang, Y., Xu, S., Li, X., Zhang, J., Sun, J., Tong, L., ... & Chen, B. (2018). Improved LRET-based detection characters of Cu^{2+} using sandwich structured $NaYF_4$@$NaYF_4$:Er^{3+}/Yb^{3+}@$NaYF_4$ nanoparticles as energy donor. Sensors and Actuators B: Chemical, 257, 829-838.